

Polarization-selective enhancement of telecom wavelength quantum dot transitions in an elliptical bullseye resonator

Andrea Barbiero,^{*,†} Ginny Shooter,[†] Tina Müller,[†] Joanna Skiba-Szymanska,[†] R. Mark Stevenson,[†] Lucy E. Goff,[‡] David A. Ritchie,[‡] and Andrew J. Shields[†]

[†]*Toshiba Europe Limited, 208 Science Park, Milton Road, Cambridge, CB4 0GZ, UK*

[‡]*Cavendish Laboratory, University of Cambridge, Madingley Road, Cambridge, CB3 0HE, United Kingdom*

E-mail: andrea.barbiero@toshiba.eu

Abstract

Semiconductor quantum dots are promising candidates for the generation of nonclassical light. Coupling a quantum dot to a device capable of providing polarization-selective enhancement of optical transitions is highly beneficial for advanced functionalities such as efficient resonant driving schemes or applications based on optical cyclicity. Here, we demonstrate broadband polarization-selective enhancement by coupling a quantum dot emitting in the telecom O-band to an elliptical bullseye resonator. We report bright single-photon emission with a degree of linear polarization of 96%, Purcell factor of 3.9, and count rates up to 3 MHz. Furthermore, we present a measurement of two-photon interference without any external polarization filtering and demonstrate compatibility with compact Stirling cryocoolers by operating the device at temperatures up to 40 K. These results represent an important step towards practical integration of optimal quantum dot photon sources in deployment-ready setups.

Introduction

Single-photon sources are an important building block for the advancement of emerging quantum technologies such as quantum key distribution,¹⁻³ quantum metrology⁴ and quantum computing.^{5,6} For most applications, an optimal source should efficiently deliver indistinguishable single photons in a well-defined spatial and polarization mode.⁷ Among the several platforms investigated over the last decades, semiconductor quantum dots (QDs)⁸ coupled to Purcell microcavities have shown excellent quantum-optical properties (high purity and indistinguishability) and state-of-the-art performance in terms of brightness and repetition rate.⁹⁻¹² Moreover, their ability to emit directly in the telecom O-band (1260 nm - 1360 nm)^{13,14} or C-band (1530 nm - 1565 nm)^{15,16} is crucial for the development of long-distance quantum communication networks^{2,17} thanks to the low-loss windows of standard silica fibers at those wavelengths.

Multiple semiconductor devices have shown the potential to serve as optimal cavity structures for the generation of single photons at high rates.¹⁸⁻²² Among these, circular Bragg gratings (CBGs, also known as bullseye resonators)²³⁻²⁵ have recently emerged as promising candidates thanks to a unique combination of moderate Purcell enhancement and high extraction efficiency in a broad spectral range. Moreover, they do not require demanding fine features and guarantee good robustness against common imperfections, such as tilted side walls or spatial displacement of the QD emitter.²⁶⁻²⁸ Singly-charged QDs in CBGs have already shown impressive count rates and first-lens efficiencies,²⁹⁻³¹ and combining those performance with a polarization-selective enhancement^{32,33} would be beneficial for multiple applications. First, it is worth noting that the most efficient QD source currently available relies on polarization selectivity to separate the flux of single photons from the driving laser and avoid a 50% loss in the collection efficiency.²² Furthermore, a polarization-selective device can induce cycling transitions, which are a crucial ingredient for the generation of photonic cluster states with protocols based on time-bin encoded qubits.^{34,35} Finally, applications such as quantum key distribution and any interference based experiments rely on

single photons generated into a well-defined polarization state. Polarized emission from a CBG has been observed when the QD is displaced from the centre of the cavity.³⁶ However this approach, which requires accurate deterministic fabrication, may have a negative impact on the Purcell enhancement because the emitter is not positioned in the region of highest confinement. An alternative strategy relies on the introduction of a small ellipticity to break the symmetry of the cavity. The first report of a QD coupled to an elliptical Bragg grating (EBG) has already displayed impressive performance, with a Purcell factor of ~ 15.7 and a polarized single-photon efficiency of $\sim 56\%$.³⁷ Nonetheless, the operating wavelength around 880 nm prevents its integration with the existing optical fiber infrastructure, and an EBG source emitting directly in the telecom regime has not been demonstrated yet.

In this work, we report on the fabrication of EBG cavities operating in the telecom O-band. By investigating the photoluminescence (PL) signal of a self-assembled InAs/GaAs QD embedded in one of those devices we demonstrate that the cavity strongly enhances one of the two orthogonal polarization components, resulting in bright single-photon emission with a degree of linear polarization $> 96\%$, Purcell factor of 3.9, and count rates up to 3 MHz. To demonstrate the effect of strong polarization selective enhancement, we report a measurement of two-photon interference without any external polarization filtering. Finally, we show stable operation of the linearly polarized single-photon source up to a temperature of 40 K for compatibility with state-of-the-art compact cryocoolers.

Results and Discussion

Similarly to conventional bullseye cavities, an elliptical Bragg grating consists of concentric periodic trenches etched in a semiconductor membrane around a central disk containing the QD emitter (Figure 1a). This device also includes an insulating SiO₂ layer and a backside Au mirror, which eliminates the downwards leakage of photons into the substrate. However, the circular symmetry of the nanostructure is broken by introducing a small ellipticity (Figure

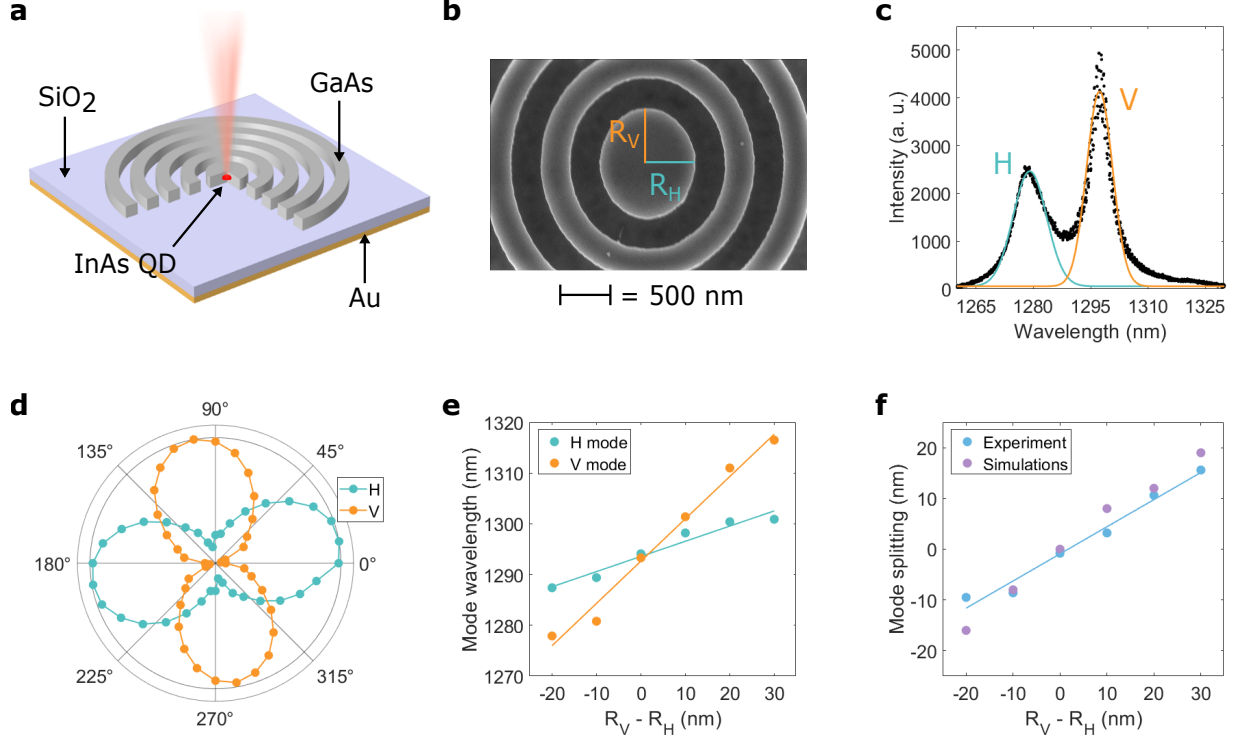


Figure 1: Structure and characterization of the elliptical Bragg grating cavities. (a) Illustration of the EBG device with a single InAs QD in the center of the cavity, an insulating SiO₂ layer and a backside Au mirror. (b) SEM top view of an exemplary EBG cavity. The labels R_H and R_V indicate the major and minor radius of the elliptical central disk, respectively. (c) Two non-degenerate cavity modes of an EBG measured under strong above-band CW laser excitation. The solid lines represent the Gaussian fit of the data. The modes are labelled H and V , with $\text{FWHM}_H = 9.68$ nm, $\text{FWHM}_V = 6.49$ nm, and a splitting of 17.73 nm. (d) Polarization-resolved measurements of the two orthogonal cavity modes. The degree of linear polarization of the H and V modes is 79.4% and 96.3%, respectively. (e) Central wavelength of the H and V modes measured on a series of 6 EBG devices with fixed $R_H = 515$ nm and variable R_V . The solid lines represent the linear fit of the data. (f) Measured splitting of the orthogonal cavity modes from (e) and corresponding values predicted by FEM simulations. The solid lines represent the linear fit of the data.

1b), which lifts the degeneracy of the fundamental cavity modes. The resulting mode splitting is proportional to the difference between the major and minor axis of the elliptical cavity.³⁷

Figure 1c shows the two non-degenerate broadband cavity modes of our main EBG device centred at 1279.69 nm (labelled H) and 1297.36 nm (labelled V), respectively. Polarization-resolved measurements (Figure 1d) confirm that the modes are orthogonally polarized, with degree of linear polarization (DLP) of 79.4% for the H mode and 96.3% for the V mode. We attribute the lower DLP of the H mode to small fabrication imperfections along the minor

axis of the elliptical cavity. To demonstrate that the separation of the modes can be easily optimized by varying the ellipticity of the device in the initial design phase, in Figure 1e we report the central wavelength of the H and V cavity modes measured on a series of 6 EBGs with fixed radius $R_H = 515$ nm and variable radius R_V . We observe that a 10 nm change in R_V leads to an 8.4 nm shift of the V mode and a 2.3 nm shift of the H mode. The latter is caused by variations in the spatial profile of the H mode when the ellipticity of the central disk is modified by varying R_V . As predicted by numerical simulations, the resulting mode splitting varies almost linearly with respect to the difference between the major and minor radius and vanishes for a circular device (Figure 1f).

When a QD transition is resonant with one of the polarized EBG modes, the cavity channels the spontaneous emission into the H and V polarizations with a ratio that depends on the mode splitting, the mode linewidth, and the Purcell factor experienced by the QD.³⁷ In Figure 2a we report the PL spectrum of a QD coupled to the V mode of our main EBG device: despite the broad nature of the bullseye cavity modes, the large splitting allows the emitted photons to be efficiently prepared in the V polarization. Polarization-resolved measurements of the integrated PL intensity (Figure 2b) confirm that the QD₁ transition displays a high DLP of 96.1% and is perfectly aligned with the V mode of the EBG. As shown by the power dependence in Figure 2c, the QD emission saturates for a CW laser power P_{sat} of approximately 1.3 μ W. After spectral filtering of the QD₁ transition, up to 3 million V polarized photon counts per second are detected by a superconducting nanowire single photon detector (SNSPD) with an efficiency of $\sim 65\%$. For comparison, less than 100 000 photons counts per second are detected in the H polarization.

The Purcell enhancement provided by the EBG cavity is quantified by measuring the radiative lifetimes under above-band pulsed excitation. In Figure 2d we compare the time-resolved luminescence trace of QD₁, which decays with a time constant $\tau_{QD1} \sim 402$ ps, to the one of a reference quantum dot in an unpatterned region of the sample. Assuming a typical lifetime $\tau_{slab} = 1.594 \pm 0.254$ ns for QDs in the bare GaAs slab based on our recent

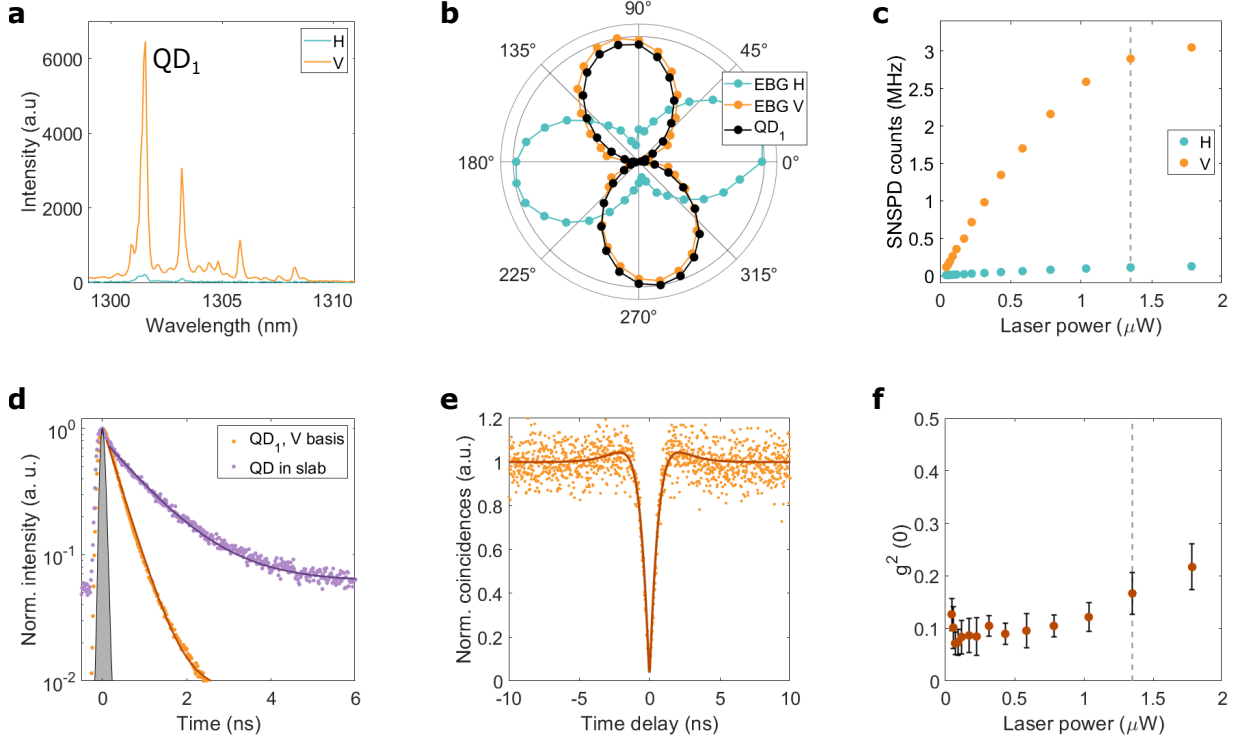


Figure 2: Characterization of the linearly polarized QD source. (a) Photoluminescence spectrum of a QD embedded in the EBG cavity. The brightest transition at 1301.5 nm is labelled QD₁. Photons are collected in the *H* and *V* polarizations. (b) Polarization-resolved photoluminescence intensity of the QD₁ transition, which is aligned with the *V* mode of the EBG and shows a degree of linear polarization of 96.1%. (c) SNSPD count rate for the *H* and *V* components of the QD₁ transition as a function of the pump power. The dashed line marks the value of CW pump power chosen as P_{sat} . (d) Radiative lifetime of the QD₁ transition (~ 402 ps) and of a reference QD transition in the unetched GaAs slab (~ 1.21 ns) measured under pulsed excitation at 80 MHz. The gray area indicates the instrument response function, while the solid lines represent the exponential fit of the decay traces. (e) Second order correlation function $g^2(\tau)$ of QD₁ measured under a CW pump power of $0.5P_{sat}$. The value of the $g^2(0)$ extracted from the raw data is 0.104 ± 0.021 . Fitting the HBT data with a four-level model (solid line) yields $g^2(0) = 0.055 \pm 0.034$. (f) Values of the $g^2(0)$ extracted from the raw data as a function of the pump power. The dashed line marks the value of P_{sat} .

work on a similar sample,³⁰ we estimate a Purcell factor $F_p = 3.9 \pm 0.6$.

The purity of the EBG single-photon source is investigated using a fiber-based Hanbury Brown and Twiss (HBT) setup. As shown in Figure 2e, the second order correlation function $g^2(\tau)$ measured under a CW pump power of $0.5P_{sat}$ exhibits the typical antibunching dip at zero delay. The $g^2(0) = 0.055 \pm 0.034$ is extracted by fitting the HBT coincidences with a four-level model.³⁸ The occurrence of multiphoton events is found to increase with

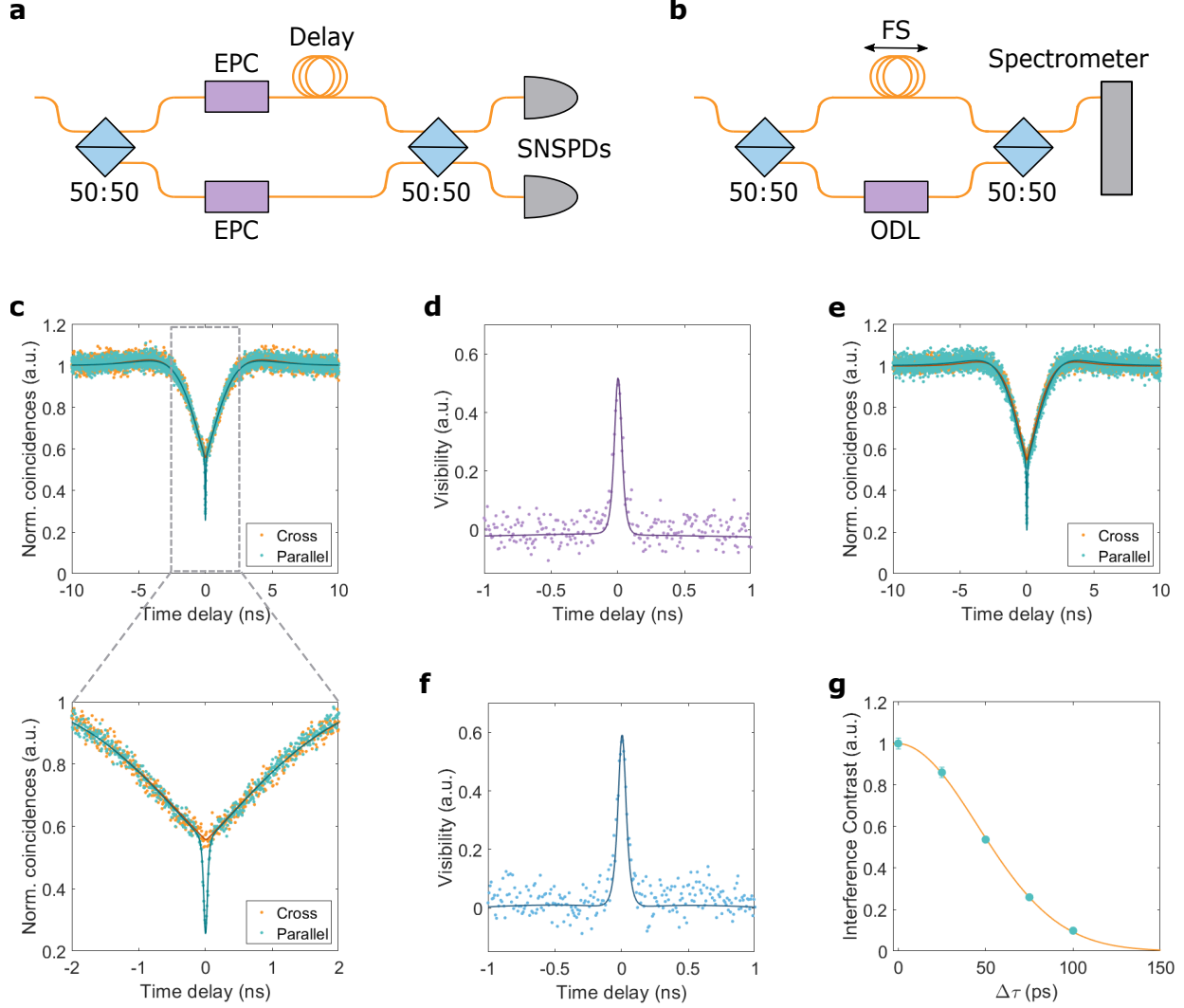


Figure 3: **Characterization of the two-photon interference (TPI).** (a) Schematic of the HOM experimental setup for TPI measurements. The polarization of photons propagating in the two arms is set by electronic polarization controllers (EPCs). Coincidences are detected by a pair of superconducting nanowire single-photon detectors. (b) Schematic of the Mach-Zehnder interferometer for coherence time measurements. One of the arms contains a fiber stretcher (FS) to generate interference fringes whereas the other one contains an optical delay line (ODL) to vary the delay between the arms on longer timescales. (c) Normalized coincidences for distinguishable (orange) and indistinguishable (teal) photons in a TPI experiment performed without any external polarization filtering. The bottom panel shows a detail of the fit on a time scale of ± 2 ns. (d) TPI visibility from (c). (e) Normalized coincidences and visibility for the same TPI experiment repeated after adding a linear polarizer in the collection arm of the microscope, which reduces the single-photon count rate by less than 5%. (f) TPI visibility from (e). (g) Coherence time of the QD₁ transition measured in a fiber-based Mach-Zehnder interferometer. Fitting the contrast decay with a Voigt profile (orange line) yields a coherence time of 63 ± 16 ps.

the excitation power (Figure 2f), due to saturation of the QD₁ transition and increased background emission.

As an example of how useful the strong polarization-selective enhancement provided by the EBG is, we now show two-photon interference (TPI) without any external polarization filtering in a fiber-based Hong-Ou-Mandel³⁹ (HOM) setup (Figure 3a). In this experiment, the expected correlations for cross-polarized (\perp) photons are given by:¹⁶

$$g_{\perp}^2(\tau) = \frac{1}{2}g^2(\tau) + \frac{1}{4} [g^2(\tau + \Delta\tau) + g^2(\tau - \Delta\tau)], \quad (1)$$

where $\Delta\tau$ is the delay between photons determined by the setup. The first term describes the probability of detecting coincidences between two photons that travel through the same arm of the interferometer, while the second term describes the expected correlations between photons that travel through different arms. In the co-polarised (\parallel) case we expect an additional interference dip at zero delay due to the HOM effect, which modifies the above equation to give:

$$g_{\parallel}^2(\tau) = \frac{1}{2}g^2(\tau) + \frac{1}{4} [g^2(\tau + \Delta\tau) + g^2(\tau - \Delta\tau)] (1 - e^{-2|\tau|/T_2}), \quad (2)$$

where T_2 is the coherence time of the QD transition. The resulting two-photon interference visibility in our setup can be calculated as:

$$V_{HOM} = 1 - \frac{g_{\parallel}^2(\tau)}{g_{\perp}^2(\tau)}. \quad (3)$$

In Figure 3c we report the measured correlations for co- and cross-polarized photons emitted by the EBG source without any external polarization filtering. From the contrast between the co- and cross-polarized coincidences at zero delay we extract a maximum raw TPI visibility $V_{HOM} = 0.543 \pm 0.023$ (Figure 3d). For comparison, Figure 3e shows the measured correlations when the residual H polarized photons are removed using a linear polarizer.

Adding external filtering increases the maximum visibility to 0.611 ± 0.032 (Figure 3f), while the loss in the single-photon count rate is limited to $< 5\%$ thanks to the high DLP displayed by the EBG source. By fitting the TPI visibility we extract a width of the interference window of 71 ps, which is similar to the coherence time $T_2 = 63 \pm 16$ ps of the QD₁ transition measured directly using a fiber-based Mach-Zehnder interferometer (Figure 3b and 3g). These values are comparable to the typical coherence times reported in literature for Stranski-Krastanov QDs emitting in the telecom O-band.^{40,41}

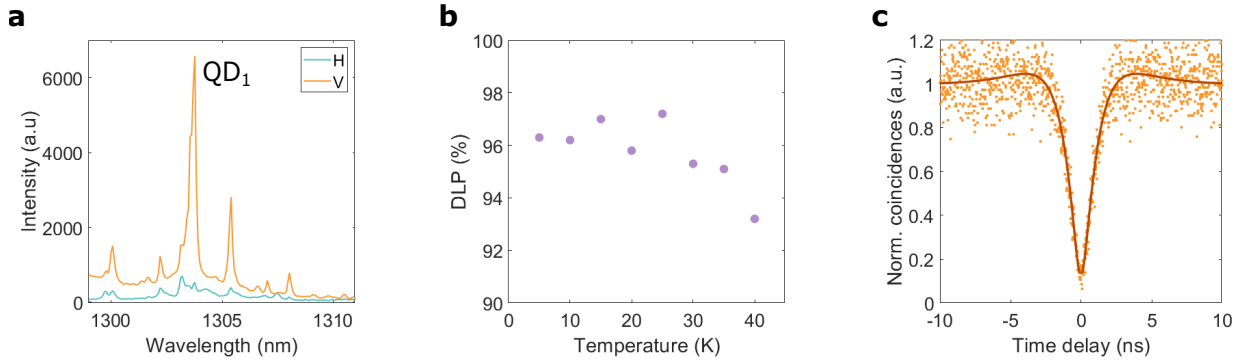


Figure 4: Performance of the linearly polarized QD source at high temperature. (a) Photoluminescence spectrum of the QD source at a temperature of 40 K. Photons are collected in the H and V polarizations. (b) Degree of linear polarization of the QD₁ transition as a function of temperature. (c) Second order correlation function $g^2(\tau)$ of QD₁ measured at a temperature of 40 K under a CW pump power of $0.3P_{sat}$. The value $g^2(0) = 0.137 \pm 0.031$ is extracted by fitting the HBT data with a four level model (solid line).

Finally, it is worth noting that QD single-photon sources operating at relatively high temperatures are most desirable for practical quantum network applications, which require not only integrability with the fiber infrastructure but also deployment outside the laboratory environment. Therefore, given the current state-of-the-art in QD operation within compact Stirling cryocoolers,^{42–44} in Figure 4 we test the performance of our EBG source at temperatures up to 40 K. Despite a ~ 3 nm redshift of the QD spectrum (Figure 4a), the broadband nature of the bullseye cavity keeps the QD₁ transition coupled to the V mode. As a result, we observe a high $DLP \geq 93\%$ in the whole range between 5 K and 40 K (Figure 4b). Operating the source in such a broad temperature range would be very challenging with narrowband devices such as micropillars, which usually require a temperature dependent optimization of

the QD-cavity coupling.⁴⁵ Moreover, the second order correlation function $g^2(\tau)$ in Figure 4c confirms that the purity of the source has not substantially deteriorated, with $g^2(0) = 0.137 \pm 0.031$.

Summary

We reported on polarization-selective enhancement of an InAs/GaAs QD emitting in the telecom O-band coupled to an elliptical Bragg grating. We designed the device to achieve a large separation between the non-degenerate cavity modes such that, thanks to a mode splitting-to-linewidth ratio close to 2, the QD emits preferentially in the V polarized mode. We took advantage of this property to demonstrate bright emission of linearly polarized single photons under above-band excitation with DLP $> 96\%$ and Purcell factor of 3.9. Furthermore, we presented a measurement of two-photon interference without any external polarization filtering and showed that the source can be operated in a broad temperature range up to 40 K with minimal impact on its polarization-selective properties, which facilitates the integration in compact modules for field deployment.

In future experiments, the H cavity mode could be exploited to resonantly excite the QD without any polarization-based laser suppression³⁷ and reveal an enhanced quality of the source in terms of purity and indistinguishability. Moreover, one could take advantage of the broadband selective enhancement provided by the EBG to generate cycling transitions without the need for QD tunability. Finally, it is worth noting that the polarized single-photon efficiency strongly depends on the Purcell factor provided by the microcavity. Higher values of F_p could be achieved by employing in-situ electron beam lithography for an optimal spatial and spectral coupling between the QD emitter and the cavity mode.

Methods

Sample growth and device fabrication

The QD sample consists of an undoped (100) GaAs substrate, a 200 nm thick $\text{Al}_{0.8}\text{Ga}_{0.2}\text{As}$ sacrificial layer, and a 240 nm thick GaAs membrane containing SK InAs QDs. After the epitaxial growth, 300 nm of SiO_2 is deposited on the surface of the GaAs slab, followed by approximately 200 nm of Au. The epitaxial wafer is then bonded to a GaAs carrier, and the original substrate and $\text{Al}_{0.8}\text{Ga}_{0.2}\text{As}$ sacrificial layer are removed using the membrane-transfer technique presented in our recent work.³⁰ Finally, the EBGs are non-deterministically fabricated on the GaAs membrane using electron-beam lithography and a chlorine-based dry etch process. The thickness of the GaAs and SiO_2 layers, and the design parameters of the EBGs are optimized using FEM numerical simulations in the frequency domain.

Optical characterization

The devices are operated at a temperature of 5 K in a closed-cycle cryostat and optically pumped using either a CW or a pulsed laser diode (80 MHz) at a wavelength of 785 nm. QD emission from a single device is collected by a fiber-coupled confocal microscope with a NA = 0.5 objective lens. For polarization-resolved measurements, a rotating half-wave plate and a fixed linear polarizer are mounted in the collection arm of the microscope. The collected photons are then sent to either a spectrometer equipped with an InGaAs photodiode array for spectral analysis, or to a tunable optical filter with 0.25 nm FWHM bandwidth in order to isolate a single transition. After spectral filtering, photons are guided to either a fiber-based HBT setup or to a HOM interferometer with electronic polarization controllers (EPCs) placed in each arm.¹⁶ Finally, photons are detected using a pair of superconducting nanowire single-photon detectors with ~ 40 ps jitter.

Author contributions

R.M.S, A.J.S and D.A.R. guided and supervised the project. L.E.G. engineered the epitaxial process and grew the sample. A.B. optimized the device design using FEM simulations. A.B. and J.S.-S. fabricated the devices. A.B. and G.S. performed the measurements. A.B. and T.M analysed the data. A.B. wrote the manuscript. All authors discussed the results and commented on the manuscript. The authors declare that they have no competing financial interests.

Acknowledgement

The authors thank D. Ellis and B. Ramsay for the PECVD SiO₂ deposition. They acknowledge funding from the Ministry of Internal Affairs and Communications, Japan, via the project of ICT priority technology (JPMI00316) ‘Research and Development for Construction of a Global Quantum Cryptography Network’. They further acknowledge funding from QFoundry (project number 48484), which is part-funded by the UK Quantum Technologies Challenge under UK Research and Innovation (UKRI).

References

- (1) Gisin, N.; Ribordy, G.; Tittel, W.; Zbinden, H. Quantum cryptography. *Reviews of Modern Physics* **2002**, *74*, 145–195.
- (2) Xu, F.; Ma, X.; Zhang, Q.; Lo, H.-K.; Pan, J.-W. Secure quantum key distribution with realistic devices. *Reviews of Modern Physics* **2020**, *92*, 131.
- (3) Couteau, C.; Barz, S.; Durt, T.; Gerrits, T.; Huwer, J.; Prevedel, R.; Rarity, J.; Shields, A.; Weihs, G. Applications of single photons to quantum communication and computing. *Nature Reviews Physics* **2023**, *5*, 326–338.

- (4) Couteau, C.; Barz, S.; Durt, T.; Gerrits, T.; Huwer, J.; Prevedel, R.; Rarity, J.; Shields, A.; Weihs, G. Applications of single photons in quantum metrology, biology and the foundations of quantum physics. *Nature Reviews Physics* **2023**, *5*, 354–363.
- (5) Kok, P.; Munro, W. J.; Nemoto, K.; Ralph, T. C.; Dowling, J. P.; Milburn, G. J. Linear optical quantum computing with photonic qubits. *Physical review A, Atomic, molecular, and optical physics* **2007**, *79*, 135–174.
- (6) Slussarenko, S.; Pryde, G. J. Photonic quantum information processing: A concise review. *Applied Physics Reviews* **2019**, *6*, 041303.
- (7) Thomas, S. E. et al. Bright Polarized Single-Photon Source Based on a Linear Dipole. *Physical review letters* **2021**, *126*, 233601.
- (8) Shields, A. J. Semiconductor quantum light sources. *Nature Photonics* **2007**, *1*, 215–223.
- (9) He, Y.-M.; He, Y.; Wei, Y.-J.; Wu, D.; Atatüre, M.; Schneider, C.; Höfling, S.; Kamp, M.; Lu, C.-Y.; Pan, J.-W. On-demand semiconductor single-photon source with near-unity indistinguishability. *Nature Nanotechnology* **2013**, *8*, 213–217.
- (10) Ding, X.; He, Y.; Duan, Z.-C.; Gregersen, N.; Chen, M.-C.; Unsleber, S.; Maier, S.; Schneider, C.; Kamp, M.; Höfling, S.; Lu, C.-Y.; Pan, J.-W. On-Demand Single Photons with High Extraction Efficiency and Near-Unity Indistinguishability from a Resonantly Driven Quantum Dot in a Micropillar. *Physical review letters* **2016**, *116*, 020401.
- (11) Senellart, P.; Solomon, G.; White, A. High-performance semiconductor quantum-dot single-photon sources. *Nature Nanotechnology* **2017**, *12*, 1026–1039.
- (12) Arakawa, Y.; Holmes, M. J. Progress in quantum-dot single photon sources for quantum information technologies: A broad spectrum overview. *Applied Physics Reviews* **2020**, *7*, 021309.

- (13) Zinoni, C.; Alloing, B.; Monat, C.; Zwiller, V.; Li, L. H.; Fiore, A.; Lunghi, L.; Gerardo, A.; de Riedmatten, H.; Zbinden, H.; Gisin, N. Time-resolved and antibunching experiments on single quantum dots at 1300nm. *Applied Physics Letters* **2006**, *88*, 691.
- (14) Ward, M. B.; Dean, M. C.; Stevenson, R. M.; Bennett, A. J.; Ellis, D.; Cooper, K.; Farrer, I.; Nicoll, C. A.; Ritchie, D. A.; Shields, A. J. Coherent dynamics of a telecom-wavelength entangled photon source. *Nature communications* **2014**, *5*, 3316.
- (15) Portalupi, S. L.; Jetter, M.; Michler, P. InAs quantum dots grown on metamorphic buffers as non-classical light sources at telecom C-band: a review. *Semiconductor Science and Technology* **2019**, *34*, 053001.
- (16) Anderson, M.; Müller, T.; Skiba-Szymanska, J.; Krysa, A. B.; Huwer, J.; Stevenson, R. M.; Heffernan, J.; Ritchie, D. A.; Shields, A. J. Coherence in single photon emission from droplet epitaxy and Stranski–Krastanov quantum dots in the telecom C-band. *Applied Physics Letters* **2021**, *118*, 014003.
- (17) Kimble, H. J. The quantum internet. *Nature* **2008**, *453*, 1023–1030.
- (18) Somaschi, N. et al. Near-optimal single-photon sources in the solid state. *Nature Photonics* **2016**, *10*, 340–345.
- (19) Gregersen, N.; McCutcheon, D. P. S.; Mørk, J.; Gérard, J.-M.; Claudon, J. A broadband tapered nanocavity for efficient nonclassical light emission. *Optics express* **2016**, *24*, 20904–20924.
- (20) Liu, F.; Brash, A. J.; O’Hara, J.; Martins, L. M. P. P.; Phillips, C. L.; Coles, R. J.; Royall, B.; Clarke, E.; Bentham, C.; Prtljaga, N.; Itskevich, I. E.; Wilson, L. R.; Skolnick, M. S.; Fox, A. M. High Purcell factor generation of indistinguishable on-chip single photons. *Nature Nanotechnology* **2018**, *13*, 835–840.

- (21) Uppu, R.; Pedersen, F. T.; Wang, Y.; Olesen, C. T.; Papon, C.; Zhou, X.; Midolo, L.; Scholz, S.; Wieck, A. D.; Ludwig, A.; Lodahl, P. Scalable integrated single-photon source. *Science advances* **2020**, *6*.
- (22) Tomm, N.; Javadi, A.; Antoniadis, N. O.; Najer, D.; Löbl, M. C.; Korsch, A. R.; Schott, R.; Valentin, S. R.; Wieck, A. D.; Ludwig, A.; Warburton, R. J. A bright and fast source of coherent single photons. *Nature Nanotechnology* **2021**, *16*, 399–403.
- (23) Davanço, M.; Rakher, M. T.; Schuh, D.; Badolato, A.; Srinivasan, K. A circular dielectric grating for vertical extraction of single quantum dot emission. *Applied Physics Letters* **2011**, *99*, 041102.
- (24) Liu, J.; Su, R.; Wei, Y.; Yao, B.; Silva, S. F. C. d.; Yu, Y.; Iles-Smith, J.; Srinivasan, K.; Rastelli, A.; Li, J.; Wang, X. A solid-state source of strongly entangled photon pairs with high brightness and indistinguishability. *Nature Nanotechnology* **2019**, *14*, 586–593.
- (25) Wang, H. et al. On-Demand Semiconductor Source of Entangled Photons Which Simultaneously Has High Fidelity, Efficiency, and Indistinguishability. *Physical review letters* **2019**, *122*, 113602.
- (26) Rickert, L.; Kupko, T.; Rodt, S.; Reitzenstein, S.; Heindel, T. Optimized designs for telecom-wavelength quantum light sources based on hybrid circular Bragg gratings. *Optics express* **2019**, *27*, 36824.
- (27) Barbiero, A.; Huwer, J.; Skiba-Szymanska, J.; Müller, T.; Stevenson, R. M.; Shields, A. J. Design study for an efficient semiconductor quantum light source operating in the telecom C-band based on an electrically-driven circular Bragg grating. *Optics express* **2022**, *30*, 10919.
- (28) Bremer, L.; Jimenez, C.; Thiele, S.; Weber, K.; Huber, T.; Rodt, S.; Herkommer, A.; Burger, S.; Höfling, S.; Giessen, H.; Reitzenstein, S. Numerical optimization of single-

- mode fiber-coupled single-photon sources based on semiconductor quantum dots. *Optics express* **2022**, *30*, 15913.
- (29) Kolatschek, S.; Nawrath, C.; Bauer, S.; Huang, J.; Fischer, J.; Sittig, R.; Jetter, M.; Portalupi, S. L.; Michler, P. Bright Purcell Enhanced Single-Photon Source in the Telecom O-Band Based on a Quantum Dot in a Circular Bragg Grating. *Nano letters* **2021**, *21*, 7740–7745.
 - (30) Barbiero, A.; Huwer, J.; Skiba-Szymanska, J.; Ellis, D. J. P.; Stevenson, R. M.; Müller, T.; Shooter, G.; Goff, L. E.; Ritchie, D. A.; Shields, A. J. High-Performance Single-Photon Sources at Telecom Wavelength Based on Broadband Hybrid Circular Bragg Gratings. *ACS Photonics* **2022**, *9*, 3060–3066.
 - (31) Nawrath, C.; Joos, R.; Kolatschek, S.; Bauer, S.; Pruy, P.; Hornung, F.; Fischer, J.; Huang, J.; Vijayan, P.; Sittig, R.; Jetter, M.; Portalupi, S. L.; Michler, P. Bright Source of Purcell–Enhanced, Triggered, Single Photons in the Telecom C–Band. *Advanced Quantum Technologies* **2023**, *5*, 104.
 - (32) Unitt, D. C.; Bennett, A. J.; Atkinson, P.; Ritchie, D. A.; Shields, A. J. Polarization control of quantum dot single-photon sources via a dipole-dependent Purcell effect. *Physical Review* **2005**, *72*, 681.
 - (33) Lee, Y.-S.; Lin, S.-D. Polarized emission of quantum dots in microcavity and anisotropic Purcell factors. *Optics express* **2014**, *22*, 1512–1523.
 - (34) Lee, J. P.; Villa, B.; Bennett, A. J.; Stevenson, R. M.; Ellis, D. J. P.; Farrer, I.; Ritchie, D. A.; Shields, A. J. A quantum dot as a source of time-bin entangled multi-photon states. *Quantum Science and Technology* **2019**, *4*, 025011.
 - (35) Appel, M. H.; Tiranov, A.; Javadi, A.; Löbl, M. C.; Wang, Y.; Scholz, S.; Wieck, A. D.; Ludwig, A.; Warburton, R. J.; Lodahl, P. Coherent Spin-Photon Interface with Waveguide Induced Cycling Transitions. *Physical review letters* **2021**, *126*, 013602.

- (36) Peniakov, G.; Buchinger, Q.; Helal, M.; Betzold, S.; Reum, Y.; Rota, M. B.; Ronco, G.; Beccaceci, M.; Krieger, T. M.; Da Silva, Saimon F. Covre.; Rastelli, A.; Trotta, R.; Pfenning, A.; Hoeffling, S.; Huber-Loyola, T. Polarized and Un-Polarized Emission from a Single Emitter in a Bullseye Resonator. *arXiv:2308.06231*
- (37) Wang, H. et al. Towards optimal single-photon sources from polarized microcavities. *Nature Photonics* **2019**, *13*, 770–775.
- (38) Anderson, M.; Müller, T.; Huwer, J.; Skiba-Szymanska, J.; Krysa, A. B.; Stevenson, R. M.; Heffernan, J.; Ritchie, D. A.; Shields, A. J. Quantum teleportation using highly coherent emission from telecom C-band quantum dots. *npj Quantum Information* **2020**, *6*, 14.
- (39) Hong, C. K.; Ou, Z. Y.; Mandel, L. Measurement of subpicosecond time intervals between two photons by interference. *Physical review letters* **1987**, *59*, 2044–2046.
- (40) Felle, M.; Huwer, J.; Stevenson, R. M.; Skiba-Szymanska, J.; Ward, M. B.; Farrer, I.; Penty, R. V.; Ritchie, D. A.; Shields, A. J. Interference with a quantum dot single-photon source and a laser at telecom wavelength. *Applied Physics Letters* **2015**, *107*, 131106.
- (41) Xiang, Z.-H.; Huwer, J.; Skiba-Szymanska, J.; Stevenson, R. M.; Ellis, D. J. P.; Farrer, I.; Ward, M. B.; Ritchie, D. A.; Shields, A. J. A tuneable telecom wavelength entangled light emitting diode deployed in an installed fibre network. *Communications Physics* **2020**, *3*, 441.
- (42) Schlehahn, A.; Krüger, L.; Gschrey, M.; Schulze, J.-H.; Rodt, S.; Strittmatter, A.; Heindel, T.; Reitzenstein, S. Operating single quantum emitters with a compact Stirling cryocooler. *The Review of scientific instruments* **2015**, *86*, 013113.
- (43) Musiał, A. et al. Plug&Play Fiber–Coupled 73 kHz Single–Photon Source Operating in the Telecom O–Band. *Advanced Quantum Technologies* **2020**, *3*, 2000018.

- (44) Gao, T.; Rickert, L.; Urban, F.; Große, J.; Srocka, N.; Rodt, S.; Musiał, A.; Żołnacz, K.; Mergo, P.; Dybka, K.; Urbańczyk, W.; Sek, G.; Burger, S.; Reitzenstein, S.; Heindel, T. A quantum key distribution testbed using a plug&play telecom-wavelength single-photon source. *Applied Physics Reviews* **2022**, *9*, 011412.
- (45) Liu, S.; Wei, Y.; Su, R.; Su, R.; Ma, B.; Chen, Z.; Ni, H.; Niu, Z.; Yu, Y.; Wei, Y.; Wang, X.; Yu, S. A deterministic quantum dot micropillar single photon source with 65% extraction efficiency based on fluorescence imaging method. *Scientific Reports* **2017**, *7*, 13986.